applied sciences

MDPI

Article

# Use of Ferritin-Based Metal-Encapsulated Nanocarriers as Anticancer Agents

**Luciana Mosca [1,*,†], Elisabetta Falvo [2,†], Pierpaolo Ceci [2], Elena Poser [1], Ilaria Genovese [1], Giulia Guarguaglini [2] and Gianni Colotti [2,*]**

1 Department of Biochemical Sciences, Sapienza University, 00185 Rome, Italy; elena.poser@uniroma1.it (E.P.); ilaria.genovese@uniroma1.it (I.G.)

2 IBPM CNR, Institute of Molecular Biology and Pathology, Italian National Research Council, 00185 Rome, Italy; elisabetta.falvo@uniroma1.it (E.F.); pierpaolo.ceci@uniroma1.it (P.C.); giulia.guarguaglini@uniroma1.it (G.G.)

* Correspondence: luciana.mosca@uniroma1.it (L.M.); gianni.colotti@uniroma1.it (G.C.); Tel.: +39-06-4991-0923 (L.M.); +39-06-4991-0910 (G.C.)

† These authors contributed equally to this work.

Academic Editor: Antonio Maffucci

Received: 24 November 2016; Accepted: 16 January 2017; Published: 21 January 2017

**Abstract:** The ability of ferritin to bind and deliver metals and metal-based drugs to human neuroblastoma SH-SY5Y cells was studied. We used heavy chain (H) ferritin-based metal-containing nanocarriers to test whether these constructs, which are able to cross the blood-brain barrier, may be used for the delivery of toxic molecules to brain cells, and to study their effect on the viability and cellular redox homeostasis of human neuroblastoma cells. We show that metal-containing nanocarriers are efficiently captured by SH-SY5Y cells. Iron-containing nanocarriers have a proliferative effect, while silver and cisplatin-encapsulated nanocarriers determine concentration-dependent neuroblastoma cell death. This work is a proof of concept for the use of ferritins for the delivery of toxic molecules to brain tumors.

**Keywords:** ferritin; cisplatin; neuroblastoma; drug delivery; targeting; metal ions; nanocarriers

## 1. Introduction

Nanocarrier (NC) systems are suitable for several applications, including cell-specific or tissue-specific drug delivery, biomedical imaging and therapy [1,2]. Many types of materials are used for the synthesis of NC: among these, special attention is given to protein cage structures, such as ferritins (Fts), because they are self-assembling, highly symmetrical proteins, with a strictly controlled size.

Fts are easy to be expressed and purified at high levels and at low costs in *Escherichia coli*, and are exceptionally stable over wide ranges of temperature and pH. Fts are small enough to penetrate capillary spaces and large enough to avoid renal clearance. Notably, Fts are physiological materials, very soluble in aqueous solutions and in the blood, with low toxicity, susceptible to chemical modifications and being modified by molecular biology techniques [3–10]. Materials such as $Fe_3O_4$, $Co_3O_4$, $Mn_3O_4$, Pt, CoPt, Pd, CdS, CdSe, ZnSe, $CaCO_3$, $SrCO_3$, Au, Ag and $BaCO_3$ have been produced and characterized in different ferritin templates [11].

Fts are the main intracellular iron storage proteins in both prokaryotes and eukaryotes, and are large (480 kDa) complexes of 24 subunits, capable of containing as many as 4500 atoms of iron ions ($Fe^{3+}$) within a hydrous ferric oxide core [12] (Figure 1). In mammals, two distinct classes of ferritin subunits exist, heavy (H) and light (L) chains, with molecular weights of about 21 kDa and 19 kDa, respectively, which share about 54% sequence identity. The H- and L-subunits have different functions,

in that the L-subunit enhances the stability of the iron core, while the H-subunit is endowed with a ferroxidase activity that is necessary for the rapid uptake of ferrous iron [13]. The H-subunit is very important for the organism because the absence of the H-ferritin (HFt) is embryonically lethal [14,15]. In contrast, bacterial ferritins contain a single subunit type that resembles the H chains [16,17].

HFt can deliver iron to many tissues, including the brain [18]. The brain imposes challenges to iron acquisition because of the highly developed tight junctions that bind neighbouring endothelial cells that make up the brain microvasculature. These junctions prevent the flux of molecules into the brain. The resulting blood-brain barrier (BBB) is a highly effective mechanism for protecting the brain from potentially harmful substances that circulate in the blood. A consequence of such a blockade, however, is that specific transport mechanisms must be designed for the trophic substances required for normal brain function. Transferrin and Fts are the main sources of iron for brain cells. Transferrin is considered the primary mechanism for cellular iron delivery to the brain, and a transferrin-mediated transport system has been identified in the BBB, based on transferrin receptors (TfRs, or CD71) [19,20]. CD71 was identified in endothelial cells in culture and in rat brain microvasculature [21].

HFt also enters the cells via CD71: upon interaction with CD71, membrane invagination takes place, with the formation of Ft-containing early endosomes [22]. HFt is, therefore, an important means for transporting iron across the BBB: in fact, iron can be delivered to the brain also in hypotransferrinemic mice [23].

CD71 expression is highly dependent on cellular iron requirement, and is increased by 1–2 orders of magnitude in malignant, metastatic and/or drug resistant tumors (for a review, see [24]). This, together with the possibility to load Ft with high amount of chemotherapeutics, and the exceptional physico-chemical properties mentioned above, makes H-subunit Ft-based nanocarriers (HFt-NCs) ideal vehicles for drug delivery to cancers [4,6]. Our group has recently synthesized Ft-based nanoparticles (NPs) designed to carry large amounts of drugs [25]. These molecules are able to bind metals and have been used against leishmaniasis [11,26].

Upon incorporation of chemotherapeutic agents, Ft-based smart nano-transporters have been developed against neoplastic cells [10,25,27]; these molecules, based on the combination of human Ft with chemotherapeutic agents (doxorubicin or cisplatin), selectively reach, recognize and kill cancer cells.

In the present study, we have exploited the ability of HFt to bind different metals, which would be scarcely soluble in aqueous media, and to deliver via TfR1/CD71 the metals and metal-based drugs to an established model of the human brain tumor, the SH-SY5Y neuroblastoma cells. We used HFt-NCs as a proof of concept to test whether these Ft constructs, which are able to pass through the BBB, may be exploited for the delivery of toxic molecules to brain cells, and to study their effect on the viability and cellular redox homeostasis of human neuroblastoma cells.

## 2. Experimental

### *2.1. Cell Culture*

The human neuroblastoma SH-SY5Y cell line was obtained from the ICLC (Genova, Italy). Cells were grown in Dulbecco's Modified Eagle Medium/Nutrient Mixture F-12 (DMEM/F-12) medium (Sigma-Aldrich Corporation, St. Louis, MO, USA) containing 10% foetal bovine serum (Gibco BRL Life Technologies Inc., Grand Island, NY, USA) and 2 mM L-glutamine (Sigma-Aldrich Corporation, St. Louis, MO, USA) at 37 °C in a humidified atmosphere of 95% air and 5% $CO_2$. Cells were plated at an appropriate density according to each experimental setting and treated with the indicated concentration of NP for different times. Appropriate controls with untreated cells or with cells treated with residual iron-containing Ft particles (see *Bacterial Expression and Purification*) were run in parallel.

### 2.2. Bacterial Expression and Purification

Recombinant human ferritin H chain (HFt) was expressed and purified from *E. coli*, as previously described [25] with the addition of one column exchange and one ultracentrifugation step. Samples dialyzed overnight against phosphate saline buffer (PBS) pH 7.5 were loaded on a strong anion exchange column HiTrap Q HP (Q Sepharose High Performance GE Healthcare, Boston, MA, USA) previously equilibrated with the same buffer. In these conditions, HFt samples eluted from the column, whereas other *E. coli* proteins and DNA contaminants did not. The recovered HFt samples were ultracentrifuged at 100,000× *g* for 55 min at 6 °C using a Beckman L8-70M ultracentrifuge (Beckman Coulter, Brea, CA, USA). The recovered supernatant was then precipitated using ammonium sulphate at 65% saturation (*w*/*v*). The pellet was resuspended and dialyzed overnight against PBS, pH 7.5, pooled, concentrated by using concentration tubes with cut-off 30 kDa Amicon Ultra-15 centrifugal filter devices, according to the manufacturer instructions (Millipore, Billerica, MA, USA), sterile filtered and stored at 4 °C. Typical yields were 100 mg of pure proteins per 1 L culture. These samples are characterized by an iron content derived from bacterial growth of about 50 atoms per protein molecule. The Fe(III) content of the samples was assessed as previously described [28].

The purity of all the preparations was assessed using Coomassie brilliant blue staining of 15% PAGE gels run in the presence of SDS. Protein concentrations were determined spectrophotometrically at 280 nm, using a molar extinction coefficient (on a 24-mer basis) of $4.56 \times 10^5$ $M^{-1} \cdot cm^{-1}$ (ProtParam sofware, https://www.expasy.org).

### 2.3. Metal-Containing Nanocarrier Preparation

Silver-containing HFt were prepared by adding $AgNO_3$ to the HFt solution (Ag/protein oligomer molar ratio 300:1) under stirring at room temperature in 10 mM HEPES-NaOH buffer at pH 7.8. After 1 h, the solution was centrifuged at 15,000× *g* for 30 min, dialyzed and concentrated using 100 kDa Amicon Ultra-15 centrifugal filter devices (Merck Millipore, Billerica, MA, USA).

The cysteine residues on the external surface of HFt were previously blocked using *N*-Ethylmaleimide (NEM)-chemistry to minimize binding of Ag(I) on the protein surface. Briefly, NEM was used at 10-fold molar excess to Cys residues of HFt in PBS pH 7.0, considering 2 Cys residues per HFt subunit (48 per 24-mer cage).

Gold-containing HFt were prepared as silver-containing ones, using $AuCl_3$ instead of $AgNO_3$.

Cisplatin-containing HFt were prepared as previously described [25]. Cisplatin (cisPt) content was quantified using a colorimetric assay based on the reaction of platinum and *o*-phenylenediamine (OPDA) [25].

Silver or gold contents were quantified as previously described [11] using graphite furnace atomic absorption spectrometry (GFAAS) and the Zeeman effect for the background correction. Protein content was quantified by a previously reported procedure [29].

### 2.4. Fluorescence Microscopy

Labeling of exposed amines of HFt with rhodamine was performed as previously described [30]. Briefly, HFt solution (2 mg/mL) was incubated with 1 mM of 5(6)-carboxytetramethylrhodamine *N*-succinimidyl ester ($\lambda_{ex}$ 552 nm, $\lambda_{em}$ 575 nm; Thermo Fisher Scientific, Waltham, MA, USA) in PBS for 2 h at pH 7.5 and room temperature under stirring in the dark. Subsequently, samples were filtered, dialyzed and exchanged with double distilled $H_2O$ and PBS by using 30 kDa Amicon Ultra-15 centrifugal filter devices to remove excess reagents. The number of dye molecules linked per protein was determined by absorbance spectroscopy, in accordance with the manufacturer's instructions, applying the Lambert-Beer law.

The cellular uptake kinetics of 0.03 mg/mL rhodamine-labeled HFt-metal by SH-SY5Y cells were determined by time-lapse video recording. Cells seeded at a density of 350,000 cells/well in 35 mm dishes (ibiTreat, cod. 81156, or glass bottom, cod. 81158, both from Ibidi, Martinsried, Germany)

or 8-well micro-slides (ibiTreat, cod. 80826, Ibidi, Martinsried, Germany) were observed under an Eclipse Ti inverted microscope (Nikon, Tokyo, Japan), using a 60× objective (Plan Apo VC 60× Oil differential interference contrast (DIC), N.A. 1.4 Nikon); during the whole observation, cells were kept in a microscope stage incubator (Basic WJ, Okolab, Pozzuoli, Italy), at 37 °C and 5% $CO_2$. DIC and fluorescence images were acquired every 20 minutes over 4 h, using a DS-Qi1Mc-U2 camera at 12 bits. Eleven z-stacks were acquired every 0.5 µm over a range of 5 µm, attenuating the fluorescence lamp intensity to 1/32. Image and movie processing were performed with the software NIS-Elements AR 4.2 (Nikon). Maximum intensity projection of nine z-stacks (for a total of 4 µm) was obtained for each image. Calculation of nanocarrier uptake was performed using the Fiji software (ImageJ, Version 2.0.0-rc-43/1.51d), by measuring mean rhodamine fluorescence in four selected areas for each cell and by subtracting the mean background fluorescence.

### 2.5. Determination of Cell Viability (MTT Reduction Assay)

Cell viability was determined by using 3-(4,5-dimethylthiazol-2-yl)-2,5-diphenyltetrazolium bromide (MTT) dye reduction assay. Briefly, cells were plated in 96-well plates at a density of 15,000 cells/well. After treatment with the indicated amount of metal-containing HFt (expressed as metal concentration), 20 µL/well of a 5 mg/mL solution of MTT (Sigma-Aldrich Corporation, St. Louis, MO, USA) in PBS was added and cells were incubated at 37 °C for 2 h. The supernatants were then aspirated off and formazan crystals were dissolved with 100 µL/well of DMSO. The optical density of each well was determined at 570 nm with a reference at 690 nm using a microplate reader (Appliskan microplate reader, Thermo Scientific, Vantaa, Finland).

### 2.6. Cell Cycle Assessment by Flow Cytometry

Cells were plated in 6-well plates at a density of 350,000 cells/well and treated for various times with the indicated amount of metal-containing HFt (expressed as metal concentration). After treatment, cells were trypsinized, collected by centrifugation and washed with PBS. The pellets were resuspended in ice-cold 70% ethanol and fixed at 4 °C for 48 h. After fixation, the cells were washed and resuspended in 600 µL of DNA staining reagent containing 180 µg/mL RNase and 50 µg/mL propidium iodide. Red fluorescence was detected by a flow cytometer (BD Accuri C6, BD Bioscences, Erembodegem, Belgium) equipped with a 488 nm excitation laser and a 585/40 nm band-pass filter (FL2 channel). The analysis was performed on 50,000 cells in each sample and the percentage of cells accumulating in the sub-G1, G0-G1, S and M peaks was calculated after appropriate gating of the cells.

### 2.7. Measurement of Intracellular Glutathione Levels

Intracellular glutathione (GSH) levels were measured by the use of the monoChloroBimane dye (mCB). Cells were seeded in 96-well plates at a density of 15,000 cells/well in complete medium without phenol red. After treatment with the indicated amount of metal-containing HFt (expressed as metal concentration), cells were stained with mCB for 1 h at 37 °C in a humidified incubator. Fluorescence was then measured in a microplate reader with a $\lambda_{ex}$ of 366 nm and a $\lambda_{em}$ of 460 nm. Blanks without mCB or without cells were run in parallel and autofluorescence subtracted to the test value. GSH intracellular levels were expressed as a percentage compared to the control cells.

### 2.8. Measurement of Mitochondrial Membrane Potential

Cells were plated in 6-well plates at a density of 350,000 cells/well and treated for various times with the indicated amounts of NPs (expressed as metal concentration). After treatment, the cells were incubated with 2.5 µg/mL JC-1 in culture medium at 37 °C for 20 min. After washing with PBS, cells were collected by trypsinization, centrifuged and washed again in PBS. Cells resuspended in PBS were analyzed by a flow cytometer equipped with band-pass filters 533/30 nm (FL1 channel) and 585/40 nm (FL2 channel), respectively. At least 50,000 events per sample were collected. Mitochondrial membrane potential ($\Delta\Psi m$) (red/green JC-1 fluorescence) was expressed as percentage of the control.

## 3. Results

### *3.1. Synthesis*

The synthesis of iron-, silver-, gold- and cisplatin-containing ferritin nanocarriers was carried out as in Methods, and high yields of stable, purified products were obtained. Silver and gold were used in the form of their metal salts in order to obtain the non-reduced metal ions directly bound to the ferritin protein. In this way, these metal ions can act directly on their targets without the need to be oxidized again intracellularly. Cisplatin was used as such as it is a standard chemotherapeutic molecule. Each type of nanocarrier contained high amounts of metal bound to the protein (Figure 1). In our hands, the metal-binding processes allowed for a content of 56 ± 3 molecules of cisPt, 104 ± 5 molecules of Au and 145 ± 5 molecules of Ag per protein molecule, respectively. The reason for this difference in loading capacity among the different metals is likely due to the relative number of binding sites present on the protein cage. All prepared solutions were very stable and able to resist unaltered for weeks at 4 °C (and for hours at 37 °C) before treatment (data not shown).

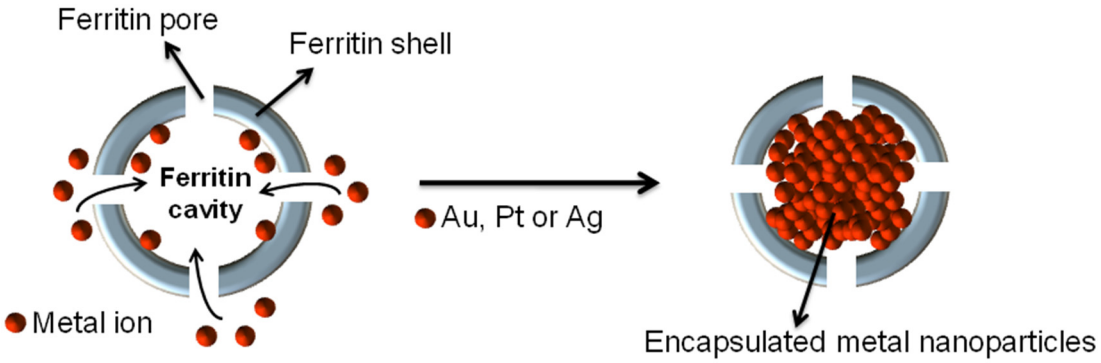


**Figure 1.** Summary of the synthesis of metal-containing human ferritin H chain (HFt)-based nanocarriers.

### *3.2. Cellular Uptake of Ferritin Nanocarriers*

The cellular uptake of rhodaminated iron-containing HFt by SH-SY5Y cells was determined by fluorescence microscopy. Figure 2A shows images taken after 0, 2, 3 and 4 h of exposure to rhodaminated HFt. The images clearly show a time-dependent increase in the intracellular red fluorescence, along with a decrease of mean background fluorescence. Part of HFt-NCs form transient aggregates in the culture medium.

Figure 2B shows the incorporation kinetics of rhodaminated HFt, where each timepoint represents mean rhodamine fluorescence intensity (AU) upon subtraction of the mean background fluorescence. The experiment shows that SH-SY5Y cells efficiently incorporate the HFt. The fitting of the timecourse shows that 50% of the plateau is reached after about 2.5 h. A video showing the cellular uptake of rhodaminated HFt is included in Supplementary Materials.

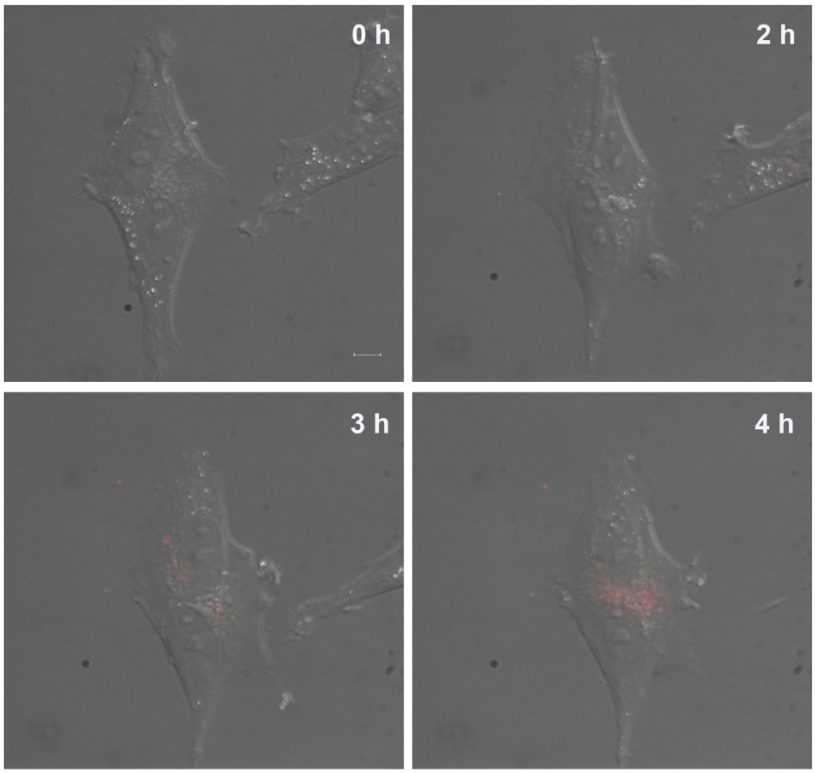


(**A**)

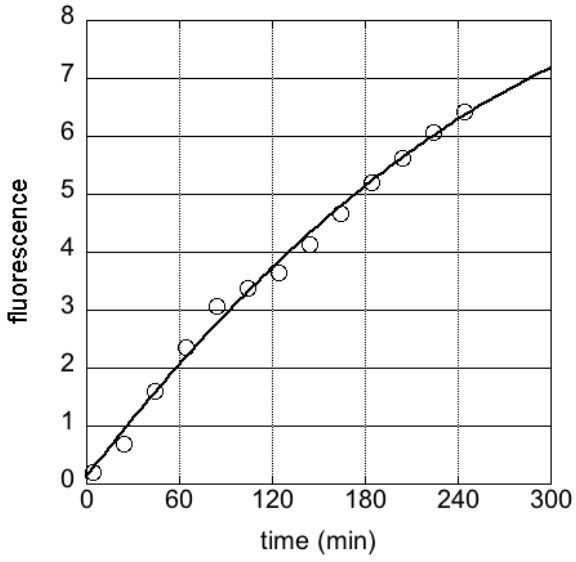


(**B**)

**Figure 2.** (**A**) time-lapse experiment of rhodaminated HFt uptake by neuroblastoma cells. SH-SY5Y cells were seeded in 8-well-plates and treated with 0.03 mg/mL rhodaminated HFt. Fluorescence images were acquired every 20 min for 4 h. Times: 0, 2, 3, 4 h (see also the Video S1 in Supplementary Materials). Scale bar: 10 μm; (**B**) timecourse of the increase in fluorescence of SH-SY5Y cells upon incubation of rhodaminated HFt. *y*-axis shows mean rhodamine fluorescence intensity (AU) measured for each cell, upon subtraction of the mean background fluorescence (average of eight cells).

### *3.3. Evaluation of Cell Viability and Cell Cycle Progression in the Presence of Metal-Containing Ferritin Nanocarriers*

Investigations were carried out to determine the effect of the different metal-containing HFt nanocarriers on the viability of SH-SY5Y cells. Figure 3 shows cellular viability in the presence of various HFt-metal concentrations, determined by the MTT assay up to 72 h. HFt (containing a small amount of iron, i.e., about 50 atoms per protein molecule) and HFt-Au (Figure 3A,B, respectively) did not show any apparent effect on cell viability up to 48 h of treatment. However, a significant proliferative effect was observed for HFt, and some effect for HFt-Au, for prolonged treatment (72 h).

Conversely, HFt-cisPt and HFt-Ag (Figure 3C,D, respectively) showed a considerable cytotoxicity as compared to HFt. In the experiments, the cell viability was negatively correlated with metal concentration in a statistically significant manner. Data reveal that after 48 h or 72 h of exposure to HFt-cisPt (Figure 3C), cell viability was reduced by about 50% when exposed to 10 μM HFt-cisPt ($p < 0.001$ vs. control), and by 60% when HFt-cisPt were present at a final concentration of 30 μM ($p < 0.001$ vs. control). The IC50 value for HFt-cisPt was 10 μM after 48 h of treatment, and 8 μM after 72 h of treatment; these experiments indicated that the toxic effect of HFt-cisPt is mostly reached within 48 h-treatments.

HFt-Ag (Figure 3D) had a dramatic effect on cell viability within 24 h of treatment even at very low concentrations, cell viability being lower than 30% upon incubation with 1 μM HFt-Ag. The IC50 value for HFt-Ag was 0.5 μM after 24 h of treatment; cell death is almost total after 48 h or 72 h treatments. Notably, HFt-Ag was found to be highly cytotoxic even for very short exposure periods, i.e., 2–4 h (data not shown), and the toxic effect of HFt-Ag was obtained within a shorter timespan (a few hours) with respect to HFt-cisPt. Conversely, treatment of SH-SY5Y cells with free $AgNO_3$ elicits cytotoxic effects comparable to HFt-Ag only at higher concentrations (Supplementary Figure S1).

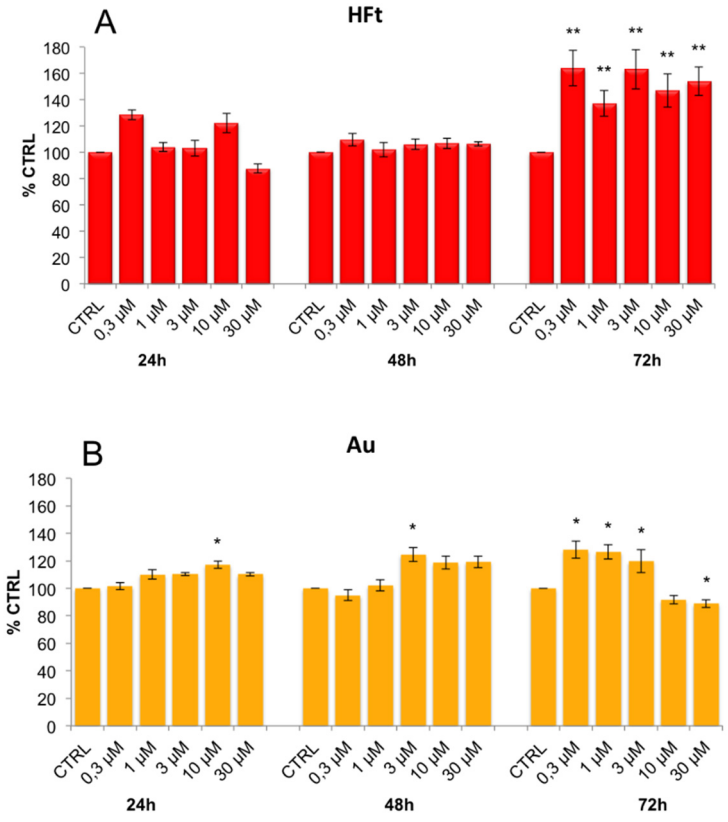


**Figure 3.** *Cont.*

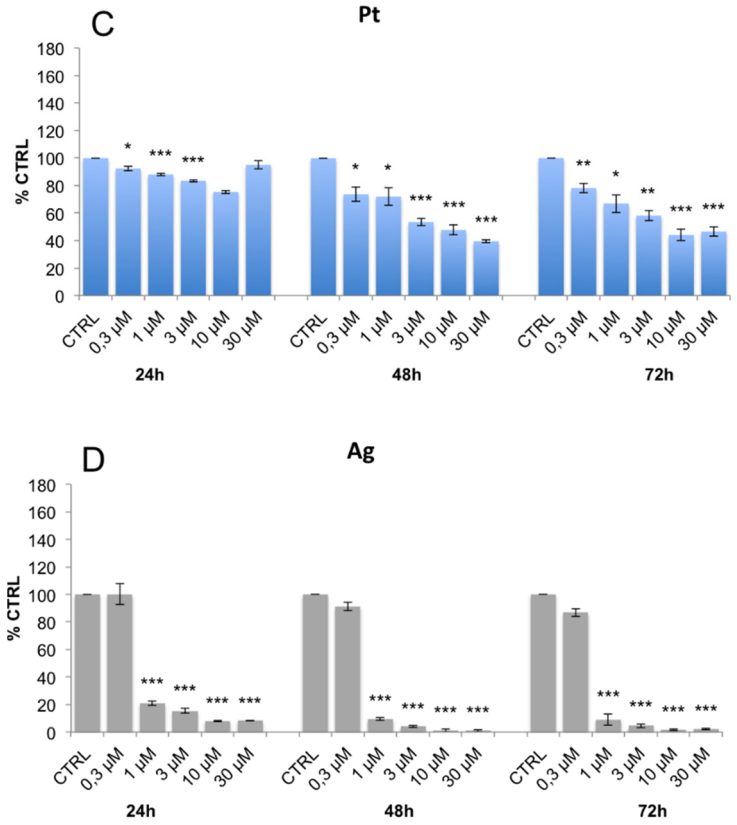


**Figure 3.** Cell viability assay on SH-SY5Ycells upon HFt-based nanocarriers exposure: (**A**): HFt; (**B**): HFt-Au; (**C**): HFt-cisPt and (**D**): HFt-Ag. For each type of nanocarrier, 24 h, 48 h and 72 h treatments with six different amounts of nanocarriers were assayed. Each series is formed by the following amounts of nanocarriers (expressed as metal concentration): control = no NCs; 0.3 µM; 1.0 µM; 3 µM; 10 µM; 30 µM. For each experimental condition, viability percentage with respect to control is shown. Each point represents the mean value of three different experiments, each of which is based on eight different points. Standard errors are indicated. Statistical significance assessed by *t*-test; * $p$ (*t*-test) < 0.05; ** $p$ (*t*-test) < 0.01; *** $p$ (*t*-test) < 0.001.

The effect of HFt-metal exposure on SH-SY5Ycells was also assayed by flow cytometry, after staining with propidium iodide dye to evaluate cell cycle progression and apoptosis. Figure 4 shows that HFt and HFt-Au do not affect cell cycle progression nor significantly modify the subG0-G1 apoptotic fraction, thus confirming our previous observations on the lack of cytotoxicity as assessed by the MTT method. Conversely, both HFt-cisPt and HFt-Ag caused a marked effect on cell cycle progression and/or cell viability. In particular, 10 µM HFt-Ag treatment induced a marked increase in the sub-G1 (hypodiploid) fraction of the total cell population, as compared with the control group, with percentages rising from about 8% to 28% at 24 h. By increasing the incubation time, most cells die upon treatment with 10 µM HFt-Ag (see Figure 3), thus impairing the analysis of the cell cycle. Treatment with 10 µM HFt-cisPt also induced a marked increase in the sub-G1 (hypodiploid) fraction of the total cell population, as compared with the control group, with percentages rising from about 9% at 24 h to 18% at 48 h and to 28% at 72 h. In the same timeframe, while the S fraction in the control group is in the 10%–12% range, it becomes about 16% at 24 h, 26% at 48 h and 23% at 72 h.

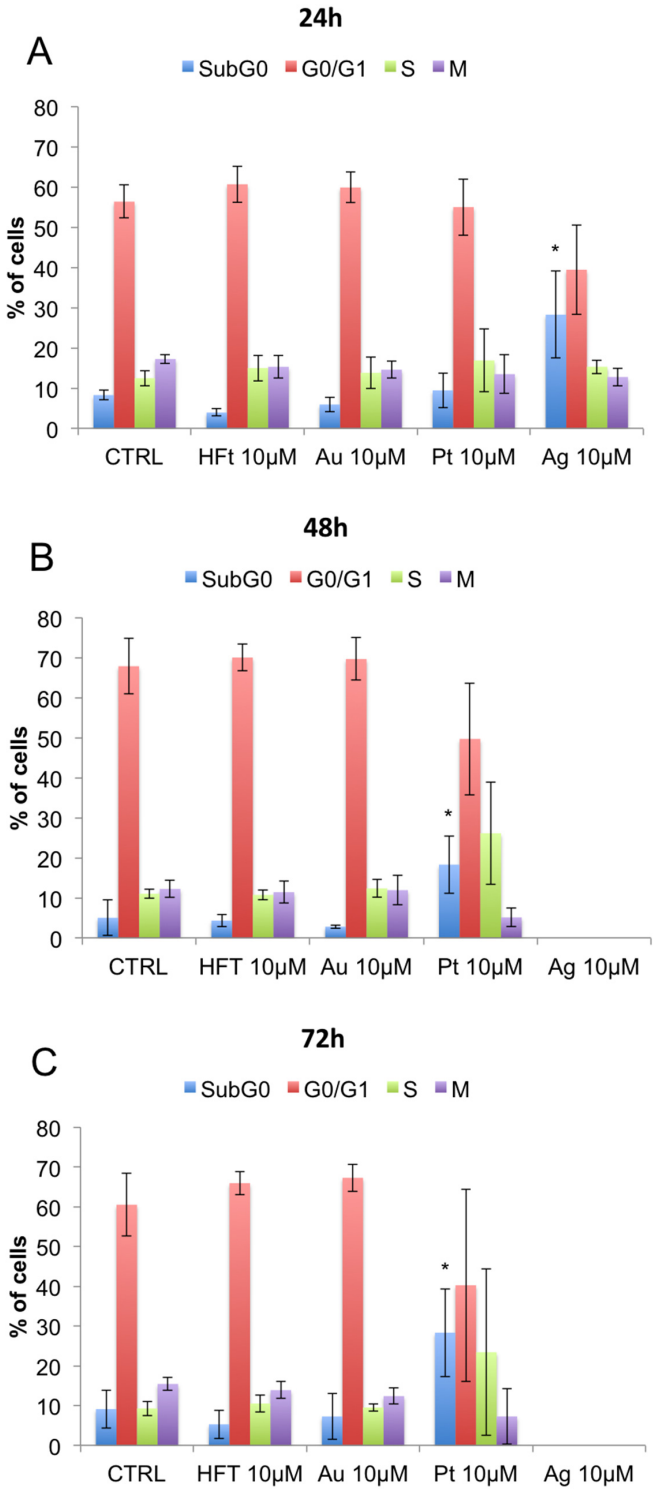


**Figure 4.** Cell cycle analysis by flow cytometry on SH-SY5Ycells upon HFt-based nanocarriers exposure, after staining with propidium iodide dye to evaluate cell cycle progression and apoptosis. (**A**) 24 h treatment; (**B**) 48 h treatment; and (**C**) 72 h treatment. For each experiment, treatments with 10 μM nanocarriers (NCs) (expressed as metal concentration) were assayed. The effects of no treatment (CTRL), treatment with HFt (CTRL), HFt-Ag, HFt-Au and HFt-cisPt are shown. Standard deviations are indicated. Statistical significance assessed by *t*-test; * $p$ (*t*-test) < 0.05.

### *3.4. Evaluation of Cellular Redox Homeostasis and Mitochondrial Transmembrane Potential in the Presence of Metal-Containing Ferritin Nanocarriers*

Previous work demonstrated that ferritin nanocarriers may induce oxidative stress-dependent damage to protein and DNA that may contribute to the toxic effect of the metal NCs [31].

The effect of the different metal-containing HFt-nanocarriers on the mitochondrial potential and on the intracellular glutathione (GSH) content of SH-SY5Y cells was then investigated. While HFt increases mitochondrial transmembrane potential after 24 and 48 h of incubation, neither treatment with HFt-cisPt nor with HFt-Au determines appreciable effects (Figure 5A). Administration of HFt-Ag dramatically destroys the mitochondrial potential, even after only 24 h of treatment.

The changes in GSH levels of SH-SY5Y cells upon administration of nanocarriers corresponding to 10 μM metal ions were also assessed (Figure 5B). HFt-Ag treatment determines fast and highly significant ($p < 0.001$) reduction of GSH content, while HFt-cisPt administration determines a small, long-term (72 h) reduction of GSH content. Surprisingly, HFt-Au treatment elicits a 30% reduction ($p < 0.05$) of GSH content within 4 h, and a remarkable long-term GSH increase of about 120% at 48 h and 72 h ($p < 0.01$).

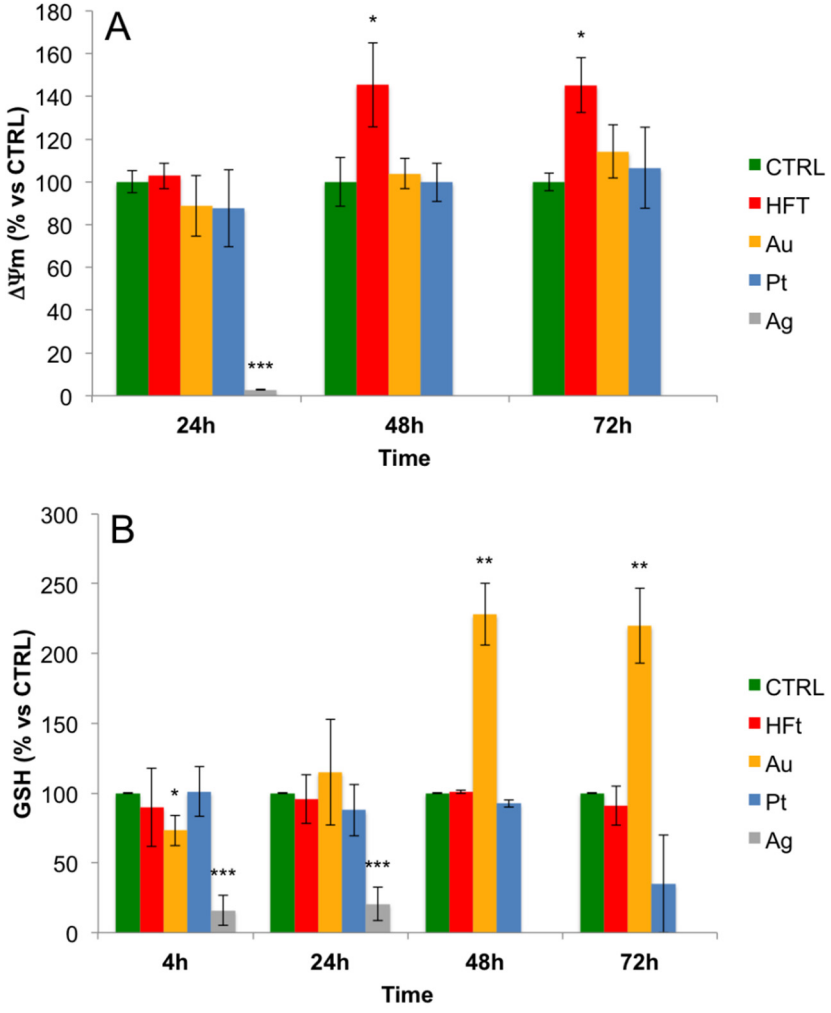


**Figure 5.** Mitochondrial potential (**A**) and glutathione (GSH) intracellular levels (**B**) of SH-SY5Y cells upon treatment for the indicated time with 10 μM nanocarriers, expressed as percentage of the control ± SD or SEM. Statistical significance assessed by *t*-test; * $p$ (*t*-test) < 0.05; ** $p$ (*t*-test) < 0.01; *** $p$ (*t*-test) < 0.001.

## 4. Discussion

The ability of HFt to pass through the BBB and to enter into cells via transferrin receptor, together with its ability to bind hundreds of metal molecules into very stable complexes, make HFt-based nanocarriers the ideal candidates for the delivery of toxic molecules to brain tumors.

In the present work, we have studied: (i) the ability of HFt to bind toxic metals into HFt-metal complexes and the efficiency of HFt-metal complexes production; (ii) the ability of HFt to enter readily into neuroblastoma SH-SY5Y cells; (iii) the differential effects of iron-, silver, gold- and cisplatin-containing HFt nanocarriers on cell viability, cell cycle, mitochondrial transmembrane potential and redox homeostasis.

We have limited the present study to metal-containing compounds in cultures of SH-SY5Y cells, and have tested the uptake of metal-containing HFt from neuroblastoma cells and the differential effect of the different metals, among which include the commonly used cisPt, on this cancer cell line.

The natural ability of HFt to bind iron was used to test the efficiency of binding of other metals and metal-containing compounds. Here, we demonstrate that HFt is able to bind efficiently high amounts (tens or even hundreds) of molecules of metal ions, and to protect them from the fast release. These materials are fully soluble in water and buffer solutions. This, together with the high yields and the overall low-cost production, makes metal-containing HFt-NCs excellent nanocarriers.

The second point tested is the ability of neuroblastoma human cells to internalize HFt-based nanocarriers from the culture medium. The level of expression of TfR1 (CD71) on the surface of cells reflects their metabolic requirements for iron [32]. Upregulation of CD71 in cancer cells is associated with malignant transformation. CD71 expression is particularly increased in metastatic and drug resistant tumors [33–38]. This makes CD71 both a tumor marker and a possible system for the delivery of small-molecule drugs to these cells by CD71-mediated endocytosis [39–44]. Recently, CD71 was identified as the receptor for HFt [22], with distinct binding sites for HFt and transferrin [45]. After binding of HFt to CD71 on the cell surface, membrane invagination takes place, and vesicles are formed. HFt is localized sequentially into endosomes and lysosomes [22]. Neuroblastoma cells, including SH-SY5Y cells, express high levels of CD71 [46,47], and are therefore able to incorporate high amounts of HFt. Molecules as sodium ascorbate, which are able to decrease the expression of CD71, cause cell death within 24 h [47].

Here, we show that SH-SY5Y neuroblastoma cells are able to incorporate HFt NCs within hours, taking advantage of their high levels of expression of transferrin receptors. This result, together with the presence of a transferrin-mediated vesicle-based transcytosis system through the BBB [19,20,48,49] makes HFt-based NCs potentially good carriers for toxic molecules to the brain tumors.

Many metals (e.g., sodium, potassium, magnesium, calcium, iron, zinc, copper, manganese, chromium, molybdenum and selenium) are required for normal biological functions in humans. We show that HFt containing small amounts of iron is not toxic, and has a slightly proliferative effect. However, most metals have toxic effects on the cells, and many metal-containing molecules are used in medicine [50], cisPt being the most commonly used in antitumor therapy. Following administration of cisPt, one of the chloride ligands is slowly displaced by water, in a process termed aquation, resulting in $[PtCl(H_2O)(NH_3)_2]^+$. Water is itself easily displaced, allowing the platinum atom to bind to DNA bases, in particular to guanine. DNA crosslinking often occurs via displacement of the other chloride ligand, typically by another guanine. CisPt-dependent DNA crosslinking interferes with cell division and elicits DNA repair mechanisms, which, in turn, activate apoptosis when repair proves impossible. Our results show that HFt-cisPt nanocarriers are good potential anti-neuroblastoma molecules: the cytotoxic effect on SH-SY5Y cells is time-dependent and concentration-dependent. As for treatment with transferrin-conjugated cisplatin [51], HFt-cisPt administration has high antiproliferative activity (IC50 = 8 μM after 72 h of treatment) and is likely to result in prolonged plasma half-life with respect to the unconjugated drug. Furthermore, treatment of SH-SY5Y cells with free cisPt elicits slightly more cytotoxic effects than HFt-cisPt at higher concentrations (above 10 μM, Supplementary Figure S1), although other studies showed cytotoxicity of cisPt only at very high concentrations (e.g., Refs. [52,53]).

Silver nanoparticles (AgNPs) have widespread applications in medicine, but there are limited studies on the potential of AgNPs as anticancer agents, such as a report on the anti-proliferative activity of AgNPs against human glioblastoma cells (U251) [54,55]. We show that HFt-Ag nanocarriers are very toxic for neuroblastoma cells, even at low concentrations, induce oxidative stress-dependent damage and determine cell death: after 48 h treatments, cell viability is <5% after treatment with 1 μM Ag. Toxicity is therefore very high at lower concentrations than those toxic upon administration of the ion alone [55]: in fact, treatment of SH-SY5Y cells with free $AgNO_3$ elicits cytotoxic effects comparable to HFt-Ag only at higher concentrations (Supplementary Figure S1). Due to this high activity, it would be important to pay particular attention to the future in vivo experiments evaluating the overall toxicity in the animal models. In fact, differently than cisplatin-based drugs, silver-based drugs for cancer have been not fully characterized to date.

HFt-Au is not cytotoxic at the concentrations used, do not affect cell cycle nor significantly modify the subGo-G1 apoptotic fraction. Even more, upon treatment with HFt-Au, the GSH content of the cells transiently decreases within 4 h of incubation, and increases in the long term, as already observed in the same cells, upon treatment with polyphenolic crude extract from *Brassica oleracea* [56]. A possible explanation is the exceptionally positive reduction potential of gold (E gold = +1.83 V, vs. silver: +0.80 V, iron: −0.44 V): therefore, HFt-Au could be able to induce a transient oxidative stress that perturbs GSH homeostasis and may cause a long-term enhanced synthesis of this peptide.

In general, the cytotoxic effect of the HFt–metal complexes is time-dependent and is strictly related to the metal release from the HFt. Although this is a slow process, the exact release mechanism of metal ions from HFt is not yet clear. It is possible that the slightly acidic pH present in the endosome and lysosome vesicles (pH 4.0–6.0) might be a stimulus to the release process. After all, the release of iron from ferritin is pH-dependent and low pH facilitates the release. In addition, the ultimate fate of the HFt is the lysosomal compartment, where the protein degradation can produce a massively metal release.

## 5. Conclusions

In conclusion, different metal-containing HFt nanocarriers, therefore, have remarkably different effects on cell viability, cell cycle, mitochondrial transmembrane potential and redox homeostasis. In particular, silver molecules bound to HFt determine neuroblastoma cell death, at lower concentrations than metal-based molecules alone. This work is a proof of concept for the use of ferritins for the delivery of toxic molecules to neuroblastoma, and paves the way for further studies on the use of H-subunit ferritin-based nanocarriers containing chemotherapeutic molecules for the cure of brain tumors.

**Supplementary Materials:** The following are available online at http://www.mdpi.com/2076-3417/7/1/101/s1, Figure S1: Cell viability assay on SH-SY5Y cells upon exposure to cytotoxic metals: $AuCl_3$ (Au); cisPt (Pt) and $AgNO_3$ (Ag). Forty-eight hours of treatment with different concentrations of metals was assayed. For each experimental condition, viability percentage with respect to control is shown. Each point represents the mean value of eight different experimental points. Standard errors are indicated, Video S1: Rhodaminated nanocarrier uptake by SH-SY5Y cells.

**Acknowledgments:** This work was supported by grants from Ateneo Sapienza 2014 and 2015 (L.M.). "Quality Methods for Design of Experiments in Scientific Research", in the FaReBio di Qualità Project: Quality and Project Management OpenLab qPMO CNR, CNCCS CNR (National Collection of Chemical Compounds and Screening Center 2015–2016), the CNR InterOmics Flagship IBISA project, the Flagship Project Nanomax: "NADINE: NAnotechnology-based Diagnostic In Neurological disease and Experimental oncology", Ministero della Salute "Ricerca Finalizzata" RF2010-131 to G.C. are acknowledged. Associazione Italiana per la Ricerca sul Cancro (AIRC) I.G. Grant 16776 to P.C. is acknowledged. We thank Drs. Valeria de Turris, Italia Anna Asteriti, Andrea Fernandez and Flavia Zanni for their invaluable technical assistance. Live cell imaging experiments were performed at the CNR-IBPM Nikon Reference Centre (Rome, Italy).

**Author Contributions:** L.M. and G.C. conceived and designed the experiments; L.M., E.F., P.C., E.P., I.G., G.G. and G.C. performed the experiments; L.M., G.G. and G.C. analyzed the data; L.M., E.F., P.C. and G.C. contributed reagents/materials/analysis tools; L.M. and G.C. wrote the paper.

**Conflicts of Interest:** The authors report no conflicts of interest.

## Abbreviations

| | |
|---|---|
| NC | nanocarriers |
| NP | nanoparticles |
| Ft | Ferritin |
| HFt | human ferritin H chain |
| TfR | transferrin receptor |
| HFt NCs | H-subunit Ft-based nanocarriers |
| GSH | glutathione |
| cisPt | cisplatin |

## References


1. Jain, R.K.; Stylianopoulos, T. Delivering nanomedicine to solid tumors. *Nat. Rev. Clin. Oncol.* **2010**, *7*, 653–664. [CrossRef] [PubMed]
2. Martinez, J.O.; Chiappini, C.; Ziemys, A.; Faust, A.M.; Kojic, M.; Liu, X.; Ferrari, M.; Tasciotti, E. Engineering multi-stage nanovectors for controlled degradation and tunable release kinetics. *Biomaterials* **2013**, *34*, 8469–8477. [CrossRef] [PubMed]
3. Geninatti Crich, S.; Bussolati, B.; Tei, L.; Grange, C.; Esposito, G.; Lanzardo, S.; Camussi, G.; Aime, S. Magnetic resonance visualization of tumor angiogenesis by targeting neural cell adhesion molecules with the highly sensitive gadolinium-loaded apoferritin probe. *Cancer Res.* **2006**, *66*, 9196–9201. [CrossRef] [PubMed]
4. Jutz, G.; van Rijn, P.; Santos Miranda, B.; Boker, A. Ferritin: A versatile building block for bionanotechnology. *Chem. Rev.* **2015**, *115*, 1653–1701. [CrossRef] [PubMed]
5. Kostiainen, M.A.; Hiekkataipale, P.; Laiho, A.; Lemieux, V.; Seitsonen, J.; Ruokolainen, J.; Ceci, P. Electrostatic assembly of binary nanoparticle superlattices using protein cages. *Nat. Nanotechnol.* **2013**, *8*, 52–56. [CrossRef] [PubMed]
6. Liang, M.; Fan, K.; Zhou, M.; Duan, D.; Zheng, J.; Yang, D.; Feng, J.; Yan, X. H-ferritin-nanocaged doxorubicin nanoparticles specifically target and kill tumors with a single-dose injection. *Proc. Natl. Acad. Sci. USA* **2014**, *111*, 14900–14905. [CrossRef] [PubMed]
7. Lin, X.; Xie, J.; Niu, G.; Zhang, F.; Gao, H.; Yang, M.; Quan, Q.; Aronova, M.A.; Zhang, G.; Lee, S.; et al. Chimeric ferritin nanocages for multiple function loading and multimodal imaging. *Nano Lett.* **2011**, *11*, 814–819. [CrossRef] [PubMed]
8. Schoonen, L.; van Hest, J.C. Functionalization of protein-based nanocages for drug delivery applications. *Nanoscale* **2014**, *6*, 7124–7141. [CrossRef] [PubMed]
9. Uchida, M.; Willits, D.A.; Muller, K.; Willis, A.F.; Jackiw, L.; Jutila, M.; Young, M.J.; Porter, A.E.; Douglas, T. Intracellular distribution of macrophage targeting ferritin-iron oxide nanocomposite. *Adv. Mater.* **2009**, *21*, 458–462. [CrossRef]
10. Falvo, E.; Tremante, E.; Arcovito, A.; Papi, M.; Elad, N.; Boffi, A.; Morea, V.; Conti, G.; Toffoli, G.; Fracasso, G.; et al. Improved doxorubicin encapsulation and pharmacokinetics of ferritin-fusion protein nanocarriers bearing proline, serine, and alanine elements. *Biomacromolecules* **2016**, *17*, 514–522. [CrossRef] [PubMed]
11. Kasyutich, O.; Ilari, A.; Fiorillo, A.; Tatchev, D.; Hoell, A.; Ceci, P. Silver ion incorporation and nanoparticle formation inside the cavity of Pyrococcus furiosus ferritin: Structural and size-distribution analyses. *J. Am. Chem. Soc.* **2010**, *132*, 3621–3627. [CrossRef] [PubMed]
12. Harrison, P.M.; Arosio, P. The ferritins: molecular properties, iron storage function and cellular regulation. *Biochim. Biophys. Acta* **1996**, *1275*, 161–203. [CrossRef]
13. Levi, S.; Santambrogio, P.; Cozzi, A.; Rovida, E.; Corsi, B.; Tamborini, E.; Spada, S.; Albertini, A.; Arosio, P. The role of the L-chain in ferritin iron incorporation. Studies of homo and heteropolymers. *J. Mol. Biol.* **1994**, *238*, 649–654. [CrossRef] [PubMed]
14. Ferreira, C.; Bucchini, D.; Martin, M.E.; Levi, S.; Arosio, P.; Grandchamp, B.; Beaumont, C. Early embryonic lethality of H ferritin gene deletion in mice. *J. Biol. Chem.* **2000**, *275*, 3021–3024. [CrossRef] [PubMed]
15. Thompson, K.; Menzies, S.; Muckenthaler, M.; Torti, F.M.; Wood, T.; Torti, S.V.; Hentze, M.W.; Beard, J.; Connor, J. Mouse brains deficient in H-ferritin have normal iron concentration but a protein profile of iron deficiency and increased evidence of oxidative stress. *J. Neurosci. Res.* **2003**, *71*, 46–63. [CrossRef] [PubMed]

16. Chiancone, E.; Ceci, P.; Ilari, A.; Ribacchi, F.; Stefanini, S. Iron and proteins for iron storage and detoxification. *Biometals* **2004**, *17*, 197–202. [CrossRef] [PubMed]
17. Wade, V.J.; Levi, S.; Arosio, P.; Treffry, A.; Harrison, P.M.; Mann, S. Influence of site-directed modifications on the formation of iron cores in ferritin. *J. Mol. Biol.* **1991**, *221*, 1443–1452. [CrossRef]
18. Fisher, J.; Devraj, K.; Ingram, J.; Slagle-Webb, B.; Madhankumar, A.B.; Liu, X.; Klinger, M.; Simpson, I.A.; Connor, J.R. Ferritin: A novel mechanism for delivery of iron to the brain and other organs. *Am. J. Physiol. Cell Physiol.* **2007**, *293*, C641–C649. [CrossRef] [PubMed]
19. Fishman, J.B.; Rubin, J.B.; Handrahan, J.V.; Connor, J.R.; Fine, R.E. Receptor-mediated transcytosis of transferrin across the blood-brain barrier. *J. Neurosci. Res.* **1987**, *18*, 299–304. [CrossRef] [PubMed]
20. Jefferies, W.A.; Brandon, M.R.; Hunt, S.V.; Williams, A.F.; Gatter, K.C.; Mason, D.Y. Transferrin receptor on endothelium of brain capillaries. *Nature* **1984**, *312*, 162–163. [CrossRef] [PubMed]
21. Kalaria, R.N. Brain microvasculature in aging. *Neurobiol. Aging* **1994**, *15*, 765–766. [CrossRef]
22. Li, L.; Fang, C.J.; Ryan, J.C.; Niemi, E.C.; Lebron, J.A.; Bjorkman, P.J.; Arase, H.; Torti, F.M.; Torti, S.V.; Nakamura, M.C.; et al. Binding and uptake of H-ferritin are mediated by human transferrin receptor-1. *Proc. Natl. Acad. Sci. USA* **2010**, *107*, 3505–3510. [CrossRef] [PubMed]
23. Malecki, E.A.; Cook, B.M.; Devenyi, A.G.; Beard, J.L.; Connor, J.R. Transferrin is required for normal distribution of $^{59}$Fe and $^{54}$Mn in mouse brain. *J. Neurol. Sci.* **1999**, *170*, 112–118. [CrossRef]
24. Tortorella, S.; Karagiannis, T.C. Transferrin receptor-mediated endocytosis: A useful target for cancer therapy. *J. Membr. Biol.* **2014**, *247*, 291–307. [CrossRef] [PubMed]
25. Falvo, E.; Tremante, E.; Fraioli, R.; Leonetti, C.; Zamparelli, C.; Boffi, A.; Morea, V.; Ceci, P.; Giacomini, P. Antibody-drug conjugates: targeting melanoma with cisplatin encapsulated in protein-cage nanoparticles based on human ferritin. *Nanoscale* **2013**, *5*, 12278–12285. [CrossRef] [PubMed]
26. Baiocco, P.; Ilari, A.; Ceci, P.; Orsini, S.; Gramiccia, M.; di Muccio, T.; Colotti, G. Inhibitory effect of silver nanoparticles on trypanothione reductase activity and leishmania infantum proliferation. *ACS Med. Chem. Lett.* **2011**, *2*, 230–233. [CrossRef] [PubMed]
27. Bellini, M.; Mazzucchelli, S.; Galbiati, E.; Sommaruga, S.; Fiandra, L.; Truffi, M.; Rizzuto, M.A.; Colombo, M.; Tortora, P.; Corsi, F.; et al. Protein nanocages for self-triggered nuclear delivery of DNA-targeted chemotherapeutics in Cancer Cells. *J. Control. Release* **2014**, *196*, 184–196. [CrossRef] [PubMed]
28. Ceci, P.; Chiancone, E.; Kasyutich, O.; Bellapadrona, G.; Castelli, L.; Fittipaldi, M.; Gatteschi, D.; Innocenti, C.; Sangregorio, C. Synthesis of iron oxide nanoparticles in Listeria innocua Dps (DNA-binding protein from starved cells): A study with the wild-type protein and a catalytic centre mutant. *Chemistry* **2010**, *16*, 709–717. [CrossRef] [PubMed]
29. Fantechi, E.; Innocenti, C.; Zanardelli, M.; Fittipaldi, M.; Falvo, E.; Carbo, M.; Shullani, V.; di Cesare Mannelli, L.; Ghelardini, C.; et al. A smart platform for hyperthermia application in cancer treatment: Cobalt-doped ferrite nanoparticles mineralized in human ferritin cages. *ACS Nano* **2014**, *8*, 4705–4719. [CrossRef] [PubMed]
30. Vannucci, L.; Falvo, E.; Failla, C.M.; Carbo, M.; Fornara, M.; Canese, R.; Cecchetti, S.; Rajsiglova, L.; Stakheev, D.; Krizan, J.; et al. In vivo targeting of cutaneous melanoma using an melanoma stimulating hormone-engineered human protein cage with fluorophore and magnetic resonance imaging tracers. *J. Biomed. Nanotechnol.* **2015**, *11*, 81–92. [CrossRef] [PubMed]
31. Alekseenko, A.V.; Waseem, T.V.; Fedorovich, S.V. Ferritin, a protein containing iron nanoparticles, induces reactive oxygen species formation and inhibits glutamate uptake in rat brain synaptosomes. *Brain Res.* **2008**, *1241*, 193–200. [CrossRef] [PubMed]
32. Gatter, K.C.; Brown, G.; Trowbridge, I.S.; Woolston, R.E.; Mason, D.Y. Transferrin receptors in human tissues: their distribution and possible clinical relevance. *J. Clin. Pathol.* **1983**, *36*, 539–545. [CrossRef] [PubMed]
33. Calzolari, A.; Oliviero, I.; Deaglio, S.; Mariani, G.; Biffoni, M.; Sposi, N.M.; Malavasi, F.; Peschle, C.; Testa, U. Transferrin receptor 2 is frequently expressed in human cancer cell lines. *Blood Cells Mol. Dis.* **2007**, *39*, 82–91. [CrossRef] [PubMed]
34. Kondo, K.; Noguchi, M.; Mukai, K.; Matsuno, Y.; Sato, Y.; Shimosato, Y.; Monden, Y. Transferrin receptor expression in adenocarcinoma of the lung as a histopathologic indicator of prognosis. *Chest* **1990**, *97*, 1367–1371. [CrossRef] [PubMed]

35. Prutki, M.; Poljak-Blazi, M.; Jakopovic, M.; Tomas, D.; Stipancic, I.; Zarkovic, N. Altered iron metabolism, transferrin receptor 1 and ferritin in patients with colon cancer. *Cancer Lett.* **2006**, *238*, 188–196. [CrossRef] [PubMed]
36. Ryschich, E.; Huszty, G.; Knaebel, H.P.; Hartel, M.; Buchler, M.W.; Schmidt, J. Transferrin receptor is a marker of malignant phenotype in human pancreatic cancer and in neuroendocrine carcinoma of the pancreas. *Eur. J. Cancer* **2004**, *40*, 1418–1422. [CrossRef] [PubMed]
37. Seymour, G.J.; Walsh, M.D.; Lavin, M.F.; Strutton, G.; Gardiner, R.A. Transferrin receptor expression by human bladder transitional cell carcinomas. *Urol. Res.* **1987**, *15*, 341–344. [CrossRef] [PubMed]
38. Singh, M.; Mugler, K.; Hailoo, D.W.; Burke, S.; Nemesure, B.; Torkko, K.; Shroyer, K.R. Differential expression of transferrin receptor (TfR) in a spectrum of normal to malignant breast tissues: implications for in situ and invasive carcinoma. *Appl. Immunohistochem. Mol. Morphol.* **2011**, *19*, 417–423. [CrossRef] [PubMed]
39. Chang, J.; Paillard, A.; Passirani, C.; Morille, M.; Benoit, J.P.; Betbeder, D.; Garcion, E. Transferrin adsorption onto PLGA nanoparticles governs their interaction with biological systems from blood circulation to brain cancer cells. *Pharm. Res.* **2012**, *29*, 1495–1505. [CrossRef] [PubMed]
40. Chiu, S.J.; Liu, S.; Perrotti, D.; Marcucci, G.; Lee, R.J. Efficient delivery of a Bcl-2-specific antisense oligodeoxyribonucleotide (G3139) via transferrin receptor-targeted liposomes. *J. Control. Release* **2006**, *112*, 199–207. [CrossRef] [PubMed]
41. Liu, G.; Mao, J.; Jiang, Z.; Sun, T.; Hu, Y.; Jiang, Z.; Zhang, C.; Dong, J.; Huang, Q.; Lan, Q. Transferrin-modified Doxorubicin-loaded biodegradable nanoparticles exhibit enhanced efficacy in treating brain glioma-bearing rats. *Cancer Biother. Radiopharm.* **2013**, *28*, 691–696. [CrossRef] [PubMed]
42. Nam, J.P.; Park, S.C.; Kim, T.H.; Jang, J.Y.; Choi, C.; Jang, M.K.; Nah, J.W. Encapsulation of paclitaxel into lauric acid-*O*-carboxymethyl chitosan-transferrin micelles for hydrophobic drug delivery and site-specific targeted delivery. *Int. J. Pharm.* **2013**, *457*, 124–135. [CrossRef] [PubMed]
43. Wu, J.; Lu, Y.; Lee, A.; Pan, X.; Yang, X.; Zhao, X.; Lee, R.J. Reversal of multidrug resistance by transferrin-conjugated liposomes co-encapsulating doxorubicin and verapamil. *J. Pharm. Pharm. Sci.* **2007**, *10*, 350–357. [PubMed]
44. Yoon, D.J.; Chu, D.S.; Ng, C.W.; Pham, E.A.; Mason, A.B.; Hudson, D.M.; Smith, V.C.; MacGillivray, R.T.; Kamei, D.T. Genetically engineering transferrin to improve its in vitro ability to deliver cytotoxins. *J. Control. Release* **2009**, *133*, 178–184. [CrossRef] [PubMed]
45. Sakamoto, S.; Kawabata, H.; Masuda, T.; Uchiyama, T.; Mizumoto, C.; Ohmori, K.; Koeffler, H.P.; Kadowaki, N.; Takaori-Kondo, A. H-ferritin is preferentially incorporated by human erythroid cells through transferrin receptor 1 in a threshold-dependent manner. *PLoS ONE* **2015**, *10*, e0139915. [CrossRef] [PubMed]
46. Lee, S.Y.; Patton, S.M.; Henderson, R.J.; Connor, J.R. Consequences of expressing mutants of the hemochromatosis gene (HFE) into a human neuronal cell line lacking endogenous HFE. *FASEB J.* **2007**, *21*, 564–576. [CrossRef] [PubMed]
47. Carosio, R.; Zuccari, G.; Orienti, I.; Mangraviti, S.; Montaldo, P.G. Sodium ascorbate induces apoptosis in neuroblastoma cell lines by interfering with iron uptake. *Mol. Cancer* **2007**, *6*, 55. [CrossRef] [PubMed]
48. Descamps, L.; Dehouck, M.P.; Torpier, G.; Cecchelli, R. Receptor-mediated transcytosis of transferrin through blood-brain barrier endothelial cells. *Am. J. Physiol.* **1996**, *270*, H1149–H1158. [PubMed]
49. Lajoie, J.M.; Shusta, E.V. Targeting receptor-mediated transport for delivery of biologics across the blood-brain barrier. *Ann. Rev. Pharmacol. Toxicol.* **2015**, *55*, 613–631. [CrossRef] [PubMed]
50. Colotti, G.; Ilari, A.; Boffi, A.; Morea, V. Metals and metal derivatives in medicine. *Mini Rev. Med. Chem.* **2013**, *13*, 211–221. [CrossRef] [PubMed]
51. Hoshino, T.; Misaki, M.; Yamamoto, M.; Shimizu, H.; Ogawa, Y.; Toguchi, H. In vitro cytotoxicities and in vivo distribution of transferrin-platinum(II) complex. *J. Pharm. Sci.* **1995**, *84*, 216–221. [CrossRef] [PubMed]
52. D'Aguanno, S.; D'Alessandro, A.; Pieroni, L.; Roveri, A.; Zaccarin, M.; Marzano, V.; de Canio, M.; Bernardini, S.; Federici, G.; Urbani, A. New insights into neuroblastoma cisplatin resistance: a comparative proteomic and meta-mining investigation. *J. Proteome Res.* **2011**, *10*, 416–428. [CrossRef] [PubMed]
53. Sun, Y.X.; Yang, J.; Wang, P.Y.; Li, Y.J.; Xie, S.Y.; Sun, R.P. Cisplatin regulates SH-SY5Y cell growth through downregulation of BDNF via miR-16. *Oncol. Rep.* **2013**, *30*, 2343–2349. [PubMed]
54. Asharani, P.V.; Hande, M.P.; Valiyaveettil, S. Anti-proliferative activity of silver nanoparticles. *BMC Cell Biol.* **2009**, *10*, 65. [CrossRef] [PubMed]

55. Coccini, T.; Manzo, L.; Bellotti, V.; de Simone, U. Assessment of cellular responses after short- and long-term exposure to silver nanoparticles in human neuroblastoma (SH-SY5Y) and astrocytoma (D384) cells. *Sci. World J.* **2014**, *2014*, 259765. [CrossRef] [PubMed]
56. Masci, A.; Mattioli, R.; Costantino, P.; Baima, S.; Morelli, G.; Punzi, P.; Giordano, C.; Pinto, A.; Donini, L.M.; d'Erme, M.; et al. Neuroprotective effect of brassica oleracea sprouts crude juice in a cellular model of alzheimer's disease. *Oxid. Med. Cell. Longev.* **2015**, *2015*, 781938. [CrossRef] [PubMed]